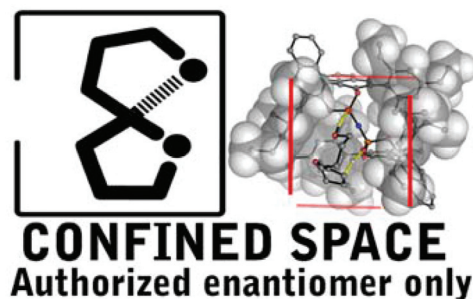


1

QM/MM study on the enantioselectivity of spiroacetalization catalysed by an imidodiphosphoric acid catalyst: how confinement works

Luis Simón* and Robert S. Paton*

An explanation of why confined imidodiphosphoric acid catalyst succeeds where other chiral phosphoric acid catalysts fail.



Please check this proof carefully. **Our staff will not read it in detail after you have returned it.**

Translation errors between word-processor files and typesetting systems can occur so the whole proof needs to be read. Please pay particular attention to: tabulated material; equations; numerical data; figures and graphics; and references. If you have not already indicated the corresponding author(s) please mark their name(s) with an asterisk. Please e-mail a list of corrections or the PDF with electronic notes attached – do not change the text within the PDF file or send a revised manuscript. Corrections at this stage should be minor and not involve extensive changes. All corrections must be sent at the same time.

Please bear in mind that minor layout improvements, e.g. in line breaking, table widths and graphic placement, are routinely applied to the final version.

We will publish articles on the web as soon as possible after receiving your corrections; **no late corrections will be made.**

Please return your **final** corrections, where possible within **48 hours** of receipt, by e-mail to: obc@rsc.org

Queries for the attention of the authors

Journal: **Organic & Biomolecular Chemistry**

Paper: **c6ob00045b**

Title: **QM/MM study on the enantioselectivity of spiroacetalization catalysed by an imidodiphosphoric acid catalyst: how confinement works**

Editor's queries are marked like this [**Q1**, **Q2**, ...], and for your convenience line numbers are indicated like this [5, 10, 15, ...].

Please ensure that all queries are answered when returning your proof corrections so that publication of your article is not delayed.

Query Reference	Query	Remarks
Q1	For your information: You can cite this article before you receive notification of the page numbers by using the following format: (authors), Org. Biomol. Chem., (year), DOI: 10.1039/c6ob00045b.	
Q2	Please carefully check the spelling of all author names. This is important for the correct indexing and future citation of your article. No late corrections can be made.	
Q3	Do you wish to add an e-mail address for the corresponding author? If so, please supply the e-mail address.	
Q4	Ref. 25 and 26: Can these references be updated?	
Q5	Ref. 39: Please provide the last name for the 1st author.	

PAPER

QM/MM study on the enantioselectivity of spiroacetalization catalysed by an imidodiphosphoric acid catalyst: how confinement works†

Luis Simón^{*a} and Robert S. Paton^{*b}

Cite this: DOI: 10.1039/c6ob00045b

Received 8th January 2016,
Accepted 26th January 2016

DOI: 10.1039/c6ob00045b

www.rsc.org/obc

BINOL-phosphoric acid catalysts (BINOP) have undergone rapid developments in recent years.^{1–9} Theoretical calculations on the mechanisms of organocatalytic reactions catalysed by BINOP^{10–29} have revealed a general mode of activation, in which the catalyst acts simultaneously as a general acid (protonating the substrate) and base or H-bond acceptor (accepting an acidic proton from the substrate). These two interactions orient and anchor prochiral substrates within the catalyst's chiral pocket, enabling discrimination between diastereomeric transition state (TS) structures that lead to enantiomeric products. Synthetic modification of the BINOL-backbone and/or substituents of chiral phosphoric acid (CPA) catalysts effectively “tune” the shape of this chiral cavity. Understanding how chiral discrimination is maximized to ensure appreciable levels of asymmetric induction is critical for the optimization and design of new phosphoric acid catalysts.

The spiroacetalization of enol-ethers **1** and **2** are promoted by CPA catalysts.³⁰ With BINOP **cat-I** a >90% yield is obtained, however, the product is almost racemic. The use of **cat-II**, however, leads to a high level of stereochemical induction (Fig. 1). This C₂-symmetric imidodiphosphoric acid has been

The mechanism for the spiroacetalization of enol-ethers **1** and **2** promoted by chiral phosphoric acid (CPA) catalyst (**I**) and by chiral imidodiphosphoric acid catalyst (**II**) has been investigated by QM/MM methods. The computed levels of enantioselectivity following exhaustive conformational analysis is in close agreement with the sense and magnitude of experimental results. Small substrates fit inside catalyst **I** to yield both enantiomers, in agreement with the absence of asymmetric induction for this reaction, while for catalyst **II** chiral discrimination between TS structures is possible. Unlike reactions catalysed by CPA or CPA derivatives in which steric effects and substrate distortion controls enantioselectivity, we show that chiral discrimination results from the restricted area and direction of possible hydrogen-bonding interactions with a more confined catalyst structure.

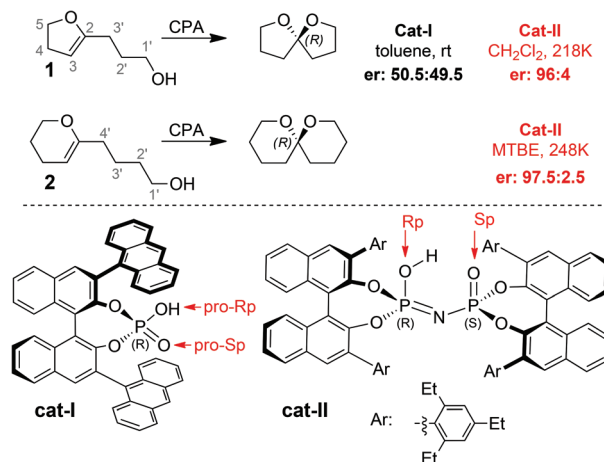


Fig. 1 Contrasting enantioselectivities in spiroacetalization due to differences in catalyst structures studied in this work. Oxygen atoms are labelled according to the absolute configuration at the attached phosphorus: in **cat-II** the Rp O is attached to the *R*-configured P atom and vice-versa. In the conjugate base of **cat-I** the O atoms are enantiotopic, and the label *pro-Rp* refers to the O atoms for which protonation results in an *R*-configured P atom and vice-versa.

^aFacultad de Ciencias Químicas, Universidad de Salamanca, Plaza de los Caídos 1-5, Salamanca E37004, Spain

^bChemistry Research Laboratory, 12 Mansfield Road, Oxford OX1 3TA, UK

†Electronic supplementary information (ESI) available: Full citation 39; analysis and justification of the relative energies of the TS structures for cat **I**. Calculation of energy barriers for stepwise reaction paths; energies and Cartesian coordinates for TS structures and intermediates. See DOI: 10.1039/c6ob00045b

developed by List.³⁰ X-ray crystal structures reveal that the environment around imidodiphosphoric group created by the 3,3'-aryl substituents imposes greater steric confinement than is the typically the case for BINOP-derived catalysts. It has also been used in the asymmetric acetalization of aldehydes with 2-hydroxymethyl-phenols,³¹ oxidation of thiols,³² Mannich

reactions,³³ Friedel–Craft reactions of indole with tosyl-
imines,³⁴ Biginelli reactions,³⁵ and asymmetric carbonyl-ene
cyclizations.³⁶ In each case a BINOP organocatalyst offers some
degree (although in some cases poor) of enantioselectivity.

In this paper, we interrogate the mechanism of spiroacetaliza-
tion for **1** and **2** catalysed by **cat-I** and **cat-II**. We focus on
how differences in size and shape of the catalysts' chiral
cavities lead to substantial differences in enantioselectivity
and enable **cat-II** to function successfully in this challenging
transformation. Previous computational studies on **II** have
been performed by Sunoj,³⁷ focussing on the asymmetric
sulfide oxidation by H₂O₂, and by List, investigating the
mechanism of the carbonyl-ene cyclizations.³⁶ In both cases,
BINOP catalysts retain some degree of enantioselectivity and
the size of the substrates (and the extent of steric interactions
with the catalyst) is considerably higher. Very recently,
Nagorny and Zimmerman³⁸ describe an experimental and
computational elucidation of the mechanism of spiroacetaliza-
tion reaction catalysed by BINOP. However, bulkier
substrates were used and confined Brønsted acid catalysts
such as **cat-II** were not considered.

Results and discussion

Computational methods

All calculations were performed with Gaussian 09.³⁹ Geometry
optimizations and TS searches employed a hybrid quantum
mechanics/molecular mechanics (QM/MM) description *via* the
ONIOM^{40–42} methodology. Atoms in the MM region are shown
in Fig. 3, 4 and 6 using a “wire”, while a “ball-and-stick” rep-
resentation is used for the QM region. The M06-2X density
functional^{43,44} with 6-31G(d,p) basis set^{45–47} was used in the
QM region and the UFF⁴⁸ force field in the MM region. The
presence of explicit UFF van der Waals terms in the MM
region delivers superior performance over a semi-empirical or
quantum chemical lower level which lack an adequate descrip-
tion of dispersion terms.^{11,15,16,20,49–53} The Gibbs free energy
was calculated at this level of theory, correcting for the errors
in entropy associated with low frequency vibrations,⁵⁴ using a
free-rotor approximation for vibrational modes below
100 cm^{–1} and a rigid rotor approximation above this cut-off as
described by Grimme.⁵⁵ M06-2X/6-311+(d,p) single point en-
ergies were evaluated for entire structures including solvation
effects by means of an IEFPCM^{56–60} calculation using the SMD
universal solvation model⁶¹ and Solvent Accessible Surface
(SAS) cavity. Parameters for diethyl-ether were used to describe
methyl *t*-butyl ether (MTBE) since these are absent in Gaussian
09, while for reactions in toluene or dichloromethane default
parameters were used. The atom-pairwise Grimme D3-dis-
persion correction with zero-damping at short range was also
included.⁶²

Unfavourable steric interactions (*i.e.* close non-bonding
contacts) between catalyst and substrate may be alleviated
through geometric distortion. To elucidate the extent of this
effect, TS geometries were re-optimized following the deletion

of 9-anthryl groups (from **cat-I**) and 2,4,6-triethylphenyl groups
(from **cat-II**). After superimposing phosphate groups, the root-
mean-squared displacement (RMSD) of the atoms in the QM
region was calculated: a lower value indicates smaller steric
distortion. Additionally, the DFT energies of the high level in
ONIOM calculations were also compared, since this term
excludes explicit energetic contributions from interactions
with the surrounding catalyst. In all figures and tables these
quantities are termed as “rmsd” and “HL”, respectively.

The bifunctional catalyst forms two key H-bonding inter-
actions (one donated, one accepted) with the substrate in each
TS. This coordination is distorted from ideal geometries to
accommodate the substrate in the chiral pocket, and we exam-
ined this distortion for each possible TS structure. Single point
energies were evaluated for each TS after deleting most of the
substrate atoms but preserving these interactions. For the
donated H-bond, all atoms were deleted except for the proton
being transferred to the substrate. The distance between this
atom and the nearest imidodiphosphoric oxygen was set to
1.4 Å (which is similar to that computed for most TS struc-
tures) but without changing bond angles or dihedrals. This
adjustment was necessary since the energy is very sensitive to
this distance. This effect is more important than in the com-
plete TS structures since the H⁺ is “naked”. The result is
referred as “H⁺ probe” in some figures and tables. The effect
of the position of the OH group that donates a H-bond to the
catalyst was tested in a similar manner, using a molecule of
methanol in an identical conformation to the substrate. This
was obtained after deleting all substrate atoms except the OH,
C1', and attached H atoms. An H atom was added at 1.07 Å
from C1'. The resulting energy is named “MeOH probe” in
figures and tables.

Solvent Accessible Surface (SAS) areas of the catalyst anions
are represented in the following discussion. This graphically
illustrates the regions of possible coordination between the
catalyst and the two protons that are attached in the spirocycli-
zation TS structures. A solvent radius of 1 Å was chosen
because the distance between interacting heteroatoms in the
catalyst and substrate was smaller than the sum of their van
der Waals radii. All figures were prepared with Pymol v0.99.⁶³

Reaction of dihydrofuran 1 promoted by cat-I. An extensive
search of possible spirocyclization conformations was per-
formed, considering different 2-3' and 1,2 torsion angles
(Fig. 2). The SAS representations of the catalyst anion show
phosphate O atoms are accessible from both sides, although it
is large in the region of negative torsion angle through the O–O
axis (in red for *pro*-Rp O, and blue for *pro*-Sp O) than in the
region of positive torsion angle (in green for *pro*-Rp O, and
yellow for *pro*-Sp O).

All possible combinations of spirocyclic TS conformers
interacting with catalyst *pro*-Rp and *pro*-Sp O atoms in the posi-
tive or negative torsion angles were considered exhaustively.
Based on previous calculations in the literature, we only con-
sidered those “bifunctional” cases in which both phosphate
oxygens were involved in the TS as H-bond acceptor or
donating.^{10–25} The results are collected in Fig. 3 and 4: the

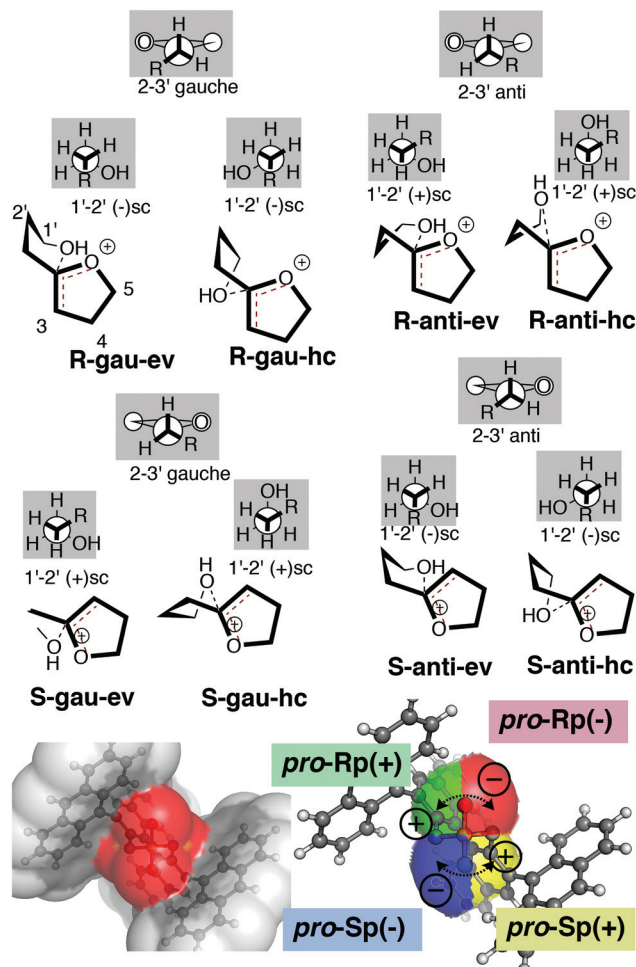


Fig. 2 Above: different possible conformations of the substrate in the spirocyclic TS; below, solvent accessible surface of cat-I conjugate base.

nomenclature describes the TS conformation, the signs of the torsion angle of the interactions with *pro*-Rp and *pro*-Sp O atoms, respectively. Analysis of the IRC for each TS showed that in most cases C3-protonation and C2...O formation are concerted such that evolution to the cyclized product occurs without an intervening intermediate. Some TS structures correspond to a step-wise mechanism in which cyclization occurs subsequently to proton-transfer. This is true of all *gau*-hc TS structures. In a recent paper, Zimmerman and Nagorny³⁸ performed dynamic studies that reveal that the intermediate is very short lived. For clarity, neither the intermediate nor the second TS structure are shown in Fig. 3, but Gibbs free energies are given in parentheses. The influence of the second TS upon the product distribution is discussed in the ESI†. In some cases, IRC analysis leads to P–O–C bond formation between catalyst and substrate. Zimmerman and Nagorny³⁸ also found anomeric phosphate intermediates, but (with a different substrate and catalyst) this mechanism was not operative due to the higher energy barrier. In our case, however, this mechanism is competitive, although it requires several bond-forming and breaking reaction steps to yield the product

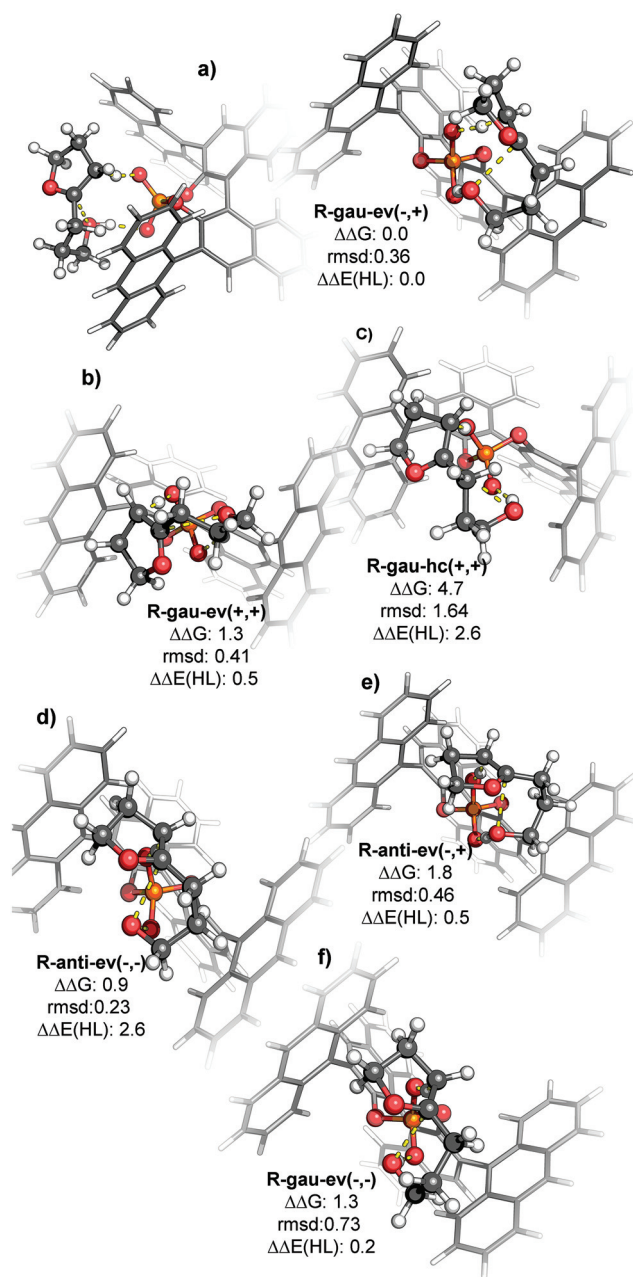


Fig. 3 Low-lying TS structures found for substrate **1** with cat-I yielding (*R*)-product.

(see details on the calculations of the reaction barriers in ESI†). All TS structures with *gau*-hc conformation correspond to any of these two latter possibilities.

For *gau*-ev, *anti*-ev and *anti*-hc conformations TS structures correspond to an asynchronous, concerted mechanism in which both proton transfer and C–O bond formation occur. The exceptions are *R-anti-ev*(–,–) and *R-anti-hc*(+,+), but in these structures the C...O bond forming distances are similar to the distances in concerted TS structures. Applying the Curtin-Hammett principle, the kinetically controlled selectivity for the irreversible spiroacetalization of **1** is computed based

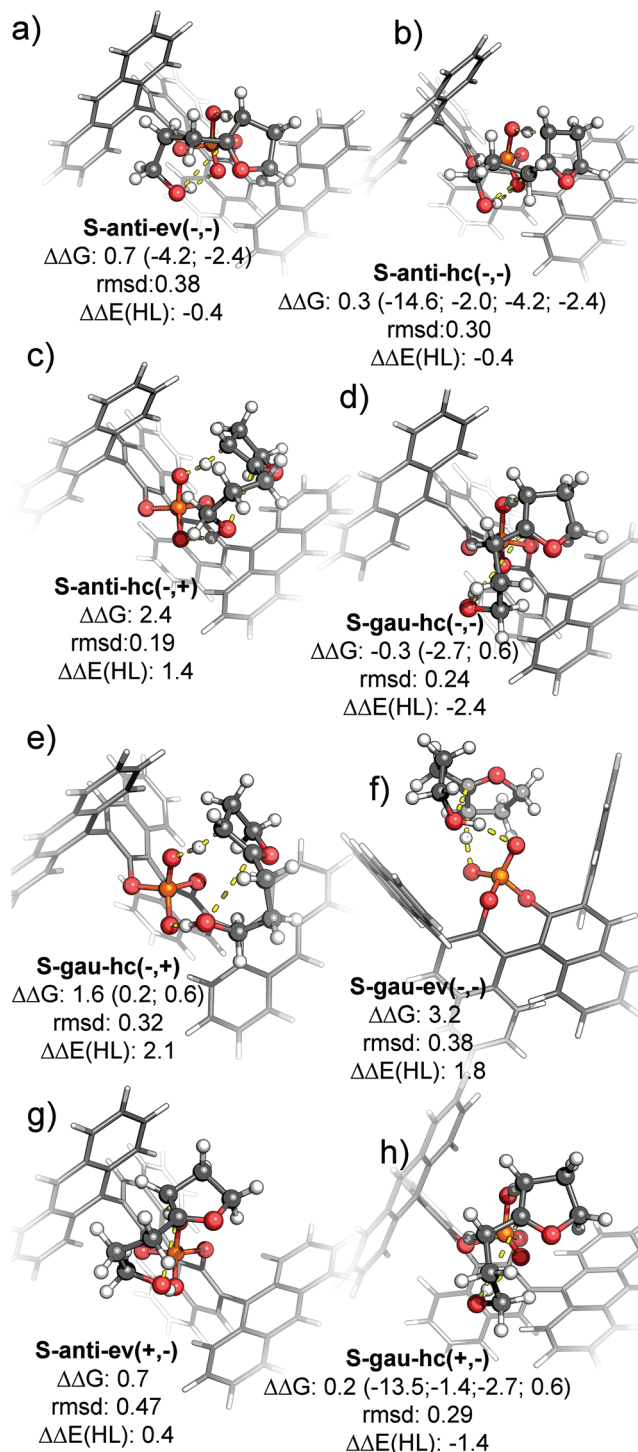


Fig. 4 Low-lying TS structures found for substrate 1 with cat-I yielding (S)-product.

on the Boltzmann factors of the ensemble of all TS structures. The computed enantiomeric ratio of 53 : 47 *S/R* is consistent with the experimentally observed near-racemic product.

The most stable TS structures are shown in Fig. 3 and 4. A detailed analysis of the reasons for the relative stability of these TS structures is included in the ESI†. In summary, cat-I

is able to find a relatively comfortable position for the substrate either in (*R*) or (*S*) yielding TS structures. Moving or rotating the substrate can prevent steric effects while the substrate is not necessarily forced to adopt unstable conformation and the orientation of H-bonds between the catalyst and the substrate can be near to optimal geometries.

Reaction of dihydrofuran 1 promoted by cat-II. Identical conformations as used in the case of cat-I were considered, but differences between the two catalysts are immediately obvious: the SAS of cat-II (Fig. 5) is noticeably reduced relative to cat-I for the region of negative torsion angle through the OO axis (in red for Rp O, and blue for Sp O), and is almost inexistent for the region of positive torsion angle (in green for Rp O, and yellow for Sp O). Also, the greater distance between the two oxygen atoms in cat-II prevents simultaneous interactions of the substrate with both negative torsion angle regions (or both positive), and accordingly only TS structures are viable with the dihydrofuran ring in the Rp(-) region and the substrate OH in the Sp(+), or with the dihydrofuran in the Rp(+) region and the OH in the Sp(-) region. These latter structures have a much higher energy due to steric effects, particularly in the case of *R* TS structures.

Results (excluding, for clarity, TS structures involving the Rp(+) region) are shown in Fig. 6; the structure names describe the conformation and the sign of the torsion angle of the interactions between the dihydrofuran with *pro*-Rp O atom. Computation of enantioselectivity based on the Boltzmann factors for the full ensemble of TS structures at the reaction temperature leads to a 95 : 5 or (*R* : *S*). This agrees well with the absolute sense and magnitude of the experimental results.

R-gau-hc(-) TS (Fig. 6a) is the most stable structure located. The dihydrofuran fits in the gap that the 2,4,6-triethylphenyl groups define in the top-right region of the catalyst, while the alcohol side chain interacts with the Sp O atom. In **R-gau-ev(-)** (+4.1 kcal mol⁻¹) and **R-anti-ev(-)** (+2.7 kcal mol⁻¹, Fig. 6b) the different C1'-C2' dihedral angle forces the dihydrofuran ring to move toward the center in a more hindered region. In agreement, the rmsd with respect to similar TS structures without the 2,4,6 triethyl-phenyl ring are higher in these structures. In **R-anti-hc(-)** TS structure (+2.5 kcal mol⁻¹, Fig. 6c) steric interactions are not more severe, but the substrate adopts a less stable conformation (C1'-C2' and C3'-C2 bonds are nearly eclipsed).

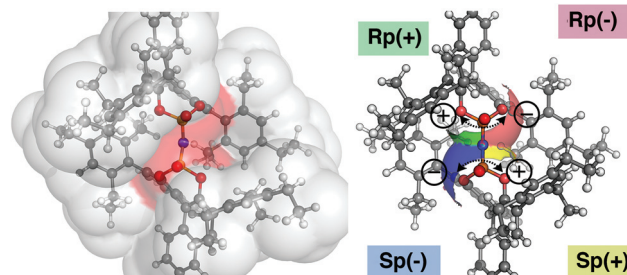


Fig. 5 The solvent accessible surface of cat-II.

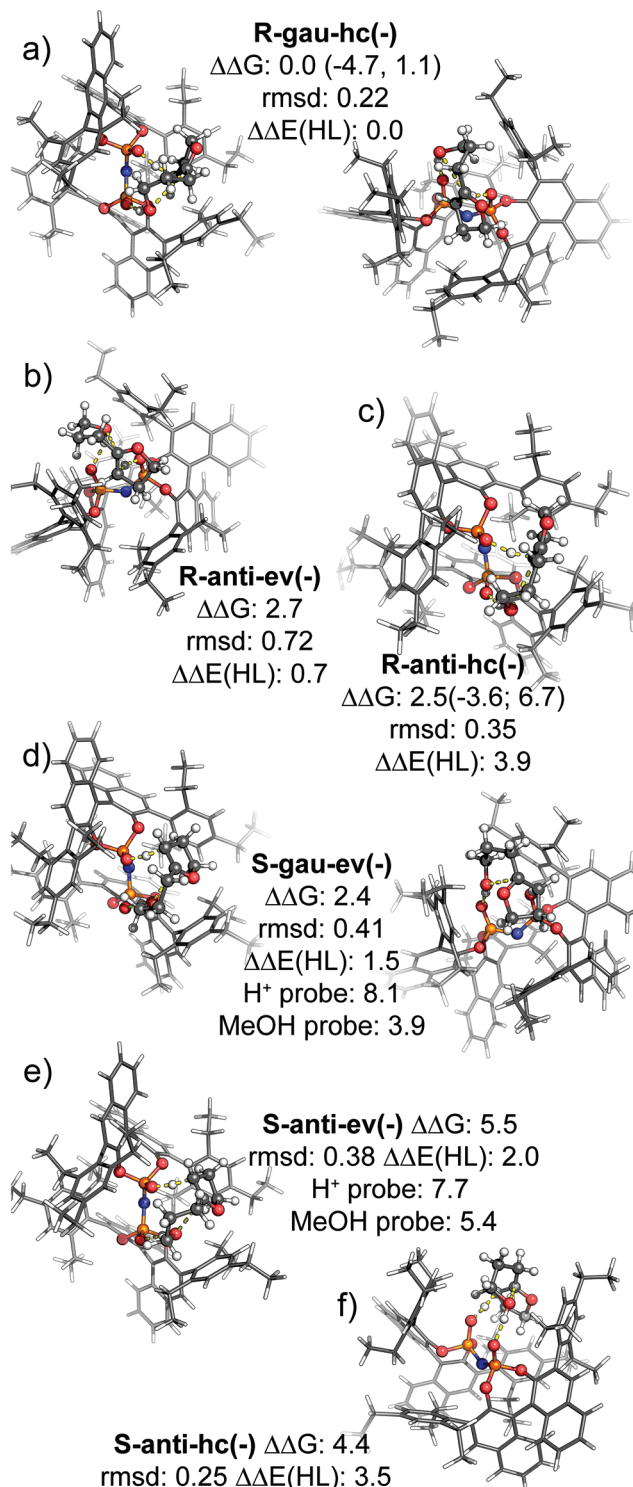


Fig. 6 Low-lying spiroacetalization TS structures of 1 catalysed by cat-II yielding (R)- and (S)-products.

Looking at the TS structures through the perspective in Fig. 5, in (S)-TS structures the furan C2, O and C4 atoms are oriented to the right. This ring can also be placed in the top-right gap preventing steric interactions, but the (P=) O...H...C2 bond changes its position: the N-P=O...H dihedral

is increased to $\approx 90^\circ$ in *S-gau-ev(-)* (+2.4 kcal mol⁻¹, Fig. 6d), *S-gau-hc(-)* (+4.4 kcal mol⁻¹), *S-anti-ev(-)* (+5.5 kcal mol⁻¹, Fig. 6e) and *S-anti-hc(-)* (+4.4 kcal mol⁻¹, Fig. 6f) from the $\approx 30^\circ$ in *R-gau-hc(-)*. This change of geometry conditions the stability of the TS structures. Single point calculations on the structure after deleting the substrate atoms (with the only modification of re-positioning the H⁺ to 1.4 Å from the phosphate oxygen, see computational methods) show a higher energy in the case of (S) TS structures. These calculations reveal that the disadvantage of (S) TS structures with respect to *R-gau-hc(-)* can be attributed to the impossibility of adopting the best dihedral N-P=O...H angle. The additional destabilization of *S-anti-hc(-)* and *S-anti-ev(-)* can be explained by the less favorable conformation of the substrate in the first (eclipsed C1'-C2' bond), and the weaker interaction with the OH group in the latter.

Reaction of dihydrofuran 2 promoted by cat-II. In forming the pyran ring for the spirocyclization of dihydropyran 2, the number of possible TS conformations is larger than for 1.⁶⁴ For each 2-4' *gauche* or *anti* conformation, it is possible to find three possible conformations of the forming tetrahydropyran ring (Fig. 7): one chair conformation (C₄) and two boat conformations (B_{1,4} and B_{2,5}). In addition, there are two possible conformations for the dihydropyran ring in which the growing C-H bond is axial/pseudo-axial: a chair and a boat conformation. Overall, it was possible to locate 48 TS structures, with 24 each leading to either (R)- or (S)-configured products (shown in the ESI†). The computed selectivity from the ensemble Boltzmann factors produces a R:S ratio of 97:3,

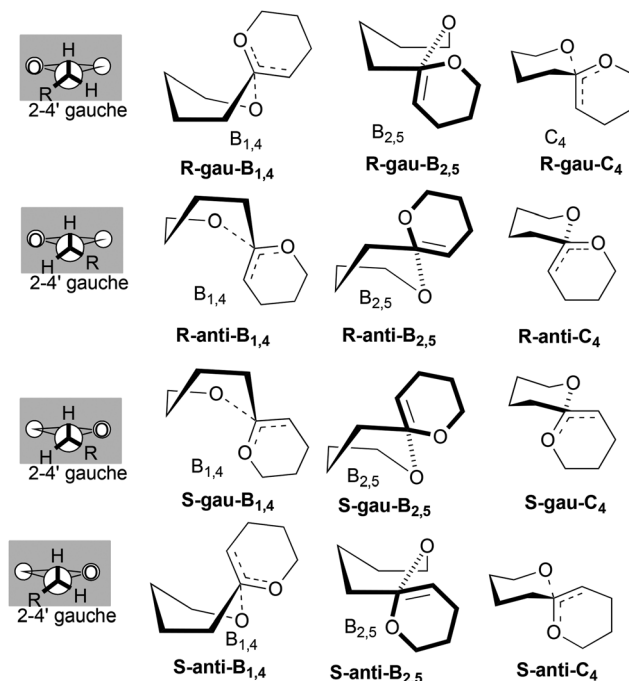


Fig. 7 Possible conformations of the forming pyran ring in the spirocyclization of 2.

again in excellent agreement with the sense and magnitude of the experimental results.

Factors dictating the stabilities of these TS structures are very similar to those already discussed for the reaction of **1**. TS structures in which the dihydropyran is in the Rp(+) region and the OH in the Sp(-) region are relatively high in energy. The most stable TS structures are very similar to those found in the reaction of **1** as revealed by pair fitting the iminodiphosphate atoms of the two structures (Fig. 8). In this case, it is also possible to relate the stability of a TS structure with the position of the dihydropyran ring: the more stable TS structures are those that are able to place this ring in the gap between the 2,4,6-triethylphenyl groups in the vicinity of Rp O atom

while maintaining the smallest N=P=O...H...C dihedral angle. Indeed, in those cases in which this dihedral is increased with respect to the reaction of **1**, (*R-anti*-B_{2,5}-C(-), *S-anti*-C₄-B(-), and *S-gau*-B_{2,5}-C(-)) the energy difference is even higher.

Comparison between cat-I and cat-II. Upon examining the TS structures obtained for both catalysts, it is immediately apparent that the confined chiral cavity in **cat-II** limits the number of the accessible TS structures. This has also been observed in the asymmetric oxidation of methyl(phenyl) sulfane catalysed by **cat-II**.³⁷ Here, even in those cases in which it is possible to find TS structures analogous to those most hindered obtained with **cat-I**, they have a very high energy. However, we emphasise that these hindered TS structures do not contribute appreciably to the Boltzmann populations of transition structures with either catalyst. The elimination of these possibilities with **cat-II** has little impact upon selectivity since this is dictated by other populated structures. A reduction in the accessible number of conformers does not contribute appreciably to the increase in asymmetric induction obtained using **cat-II**.

It is also evident that unfavourable steric interactions due to 2,4,6-triethylphenyl groups in **cat-II** are more prominent than with the 9-anthryl substituents of **cat-I** (Fig. 9). In their study, Sunoj and Jindal³⁷ observed that the origin of enantioselectivity was complementarity of more stable TS structure with the chiral pocket defined by the catalyst, apparent from comparing the degree of distortion required to accommodate TS structures leading to major and minor products. In our

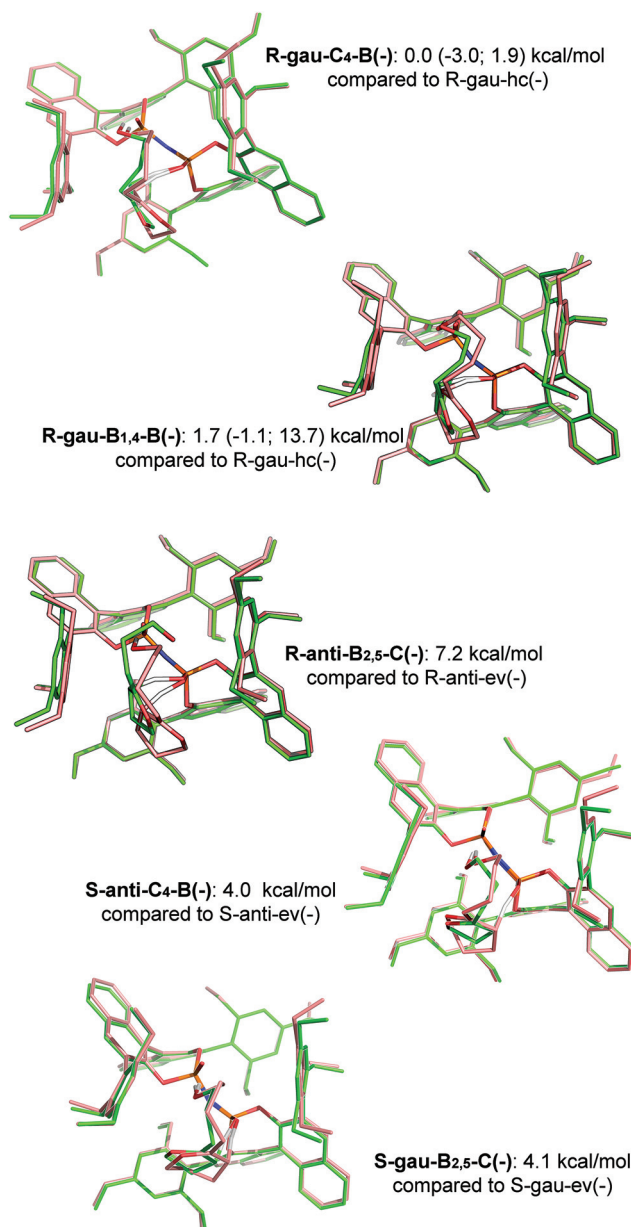


Fig. 8 The most stable TS structures for the **cat-II** promoted reaction of **2** (red), superimposed with analogous structures for **1** (green).

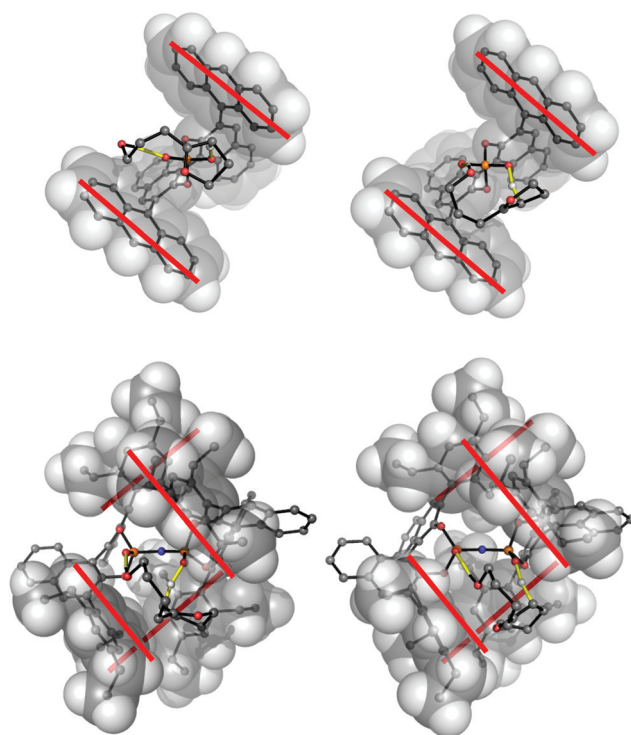


Fig. 9 Comparison between the catalytic pockets of **cat I** (top) and **II** (bottom). The two lowest TS structures are shown for each catalyst.

study, it is also clear that many TS structures suffer from steric hindrance, as revealed by the RMSD values obtaining after pair-fitting these structures with those derived after removing the 2,4,6-triethylphenyl groups. However, the reactant in this study is very small and it is possible to find TS structures leading to either enantiomer in which the dihydrofuran/pyran ring fits in a gap virtually free of steric effects.

Of particular importance to the relatively small substrates considered here, is that the catalyst cavity in confined Brønsted acid **cat-II** creates a steric environment that masks most of the area exposed by the imidodiphosphoric acid oxygens. This poses severe limits on the coordination geometries accessible for H-bonding interactions between catalyst and substrate. The difference in “availability” of the catalyst oxygen atoms is shown in Fig. 2 and 5, but it should also be noted that the SAS areas reflect accessibility but do not indicate the energetics of a particular coordination geometry. To do this we evaluated the affinity for a “probe” proton at various points on the accessible surface area.

These calculations were made from the ONIOM minimized structure of the catalyst anion. To save computational time, only the QM region of the catalyst was used in the mapping. Fig. 10a shows the surface around the oxygen atom constructed with a 1.4 Å radius. As expected, those TS structures privileged by the position of the donating H atom show this atom in a favourable region of this surface. (in Fig. 9a, this H⁺ shown for *R-anti-ev*(–) in red and *S-gau-hc*(–) in green). However, not all points around these oxygen atoms are accessible. Fig. 10b shows the surface that can be occupied by protons that accomplished simultaneously the following three conditions: (i) they are to a 1.4 ± 0.05 Å distance from catalyst oxygen; (ii) it is possible to place a C atom separated 1.3 ± 0.05 Å from it that is not closer to any other atom in the catalyst (including the MM region) more than 0.9 times the sum of the van der Waals radii (the 1.3 value was chosen because it is typically the distance for the C...H forming bond); and (iii) the (P=)O...H=C angle is between 140° and 220°, a 40° deviation from the optimal 180°. Therefore, the surface in Fig. 10b rep-

resents the points in which the H⁺ that is donated in the TS could be effectively located. This surface is considerably reduced as a consequence of the confinement, which is even more evident after comparing with a similar surface calculated for **cat I** (Fig. 10c). Deformation of the catalyst could increase this surface, but would incur the penalty of the associated distortion energy.

Conclusions

The spiroacetalization of enol-ethers **1** and **2** promoted by binol phosphoric acid catalyst **I** and imidodiphosphoric acid catalyst **II** has been studied by QM/MM methods. In the three reactions examined the calculated transition structures, based on systematic sampling over the conformational degrees of freedom, give computational selectivities in very good agreement with the sense and magnitude of asymmetric induction observed in previous experiments. Based on the high level of quantitative agreement we provide a qualitative explanation for the origin of the enantioselectivity boost observed with catalyst **II**. For CPA **I** there are many possible TS structures, and some of them can avoid unfavorable steric interactions with the catalyst anthryl-substituents while adopting stable conformations and favorable H-bonding geometries. Previous studies on the mechanism of CPA catalysed reactions show that this was not the case for bulkier substrates.^{15,16,20}

The situation is different with catalyst **II**. The number of possible TS structures is reduced since the increased steric hindrance prohibits the occurrence of TS conformations that are possible with the more open catalyst **I**. This reduction in the number of conformations, however, has little effect on selectivity since the penalized structures do contribute to the product distribution with either catalyst due to their comparative high energy. Despite the restricted confinement and increased steric demands of catalyst **II**, undistorted substrate conformations avoiding close contacts are possible for both enantiomers. The main source of chiral discrimination comes from the enforced orientation of bifunctional H-bonding interactions between the catalyst and reactant. The accessible area to the reactant of the imidodiphosphoric oxygen is considerably limited as a consequence of the “confinement”, and not all the points in this area are equally able to interact with the substrate. We hope that this observation could help to find future uses of catalyst **II** and inspire the design of new organo-catalyst for small, not sterically demanding, reactants.

Acknowledgements

We acknowledge the employment of University of Salamanca server housing service. We thank A. López García and J. A. González Ramos for IT support. RSP acknowledges the use of the EPSRC UK. National Service for Computational Chemistry Software (CHEM 773) at Imperial College London in carrying out this work.

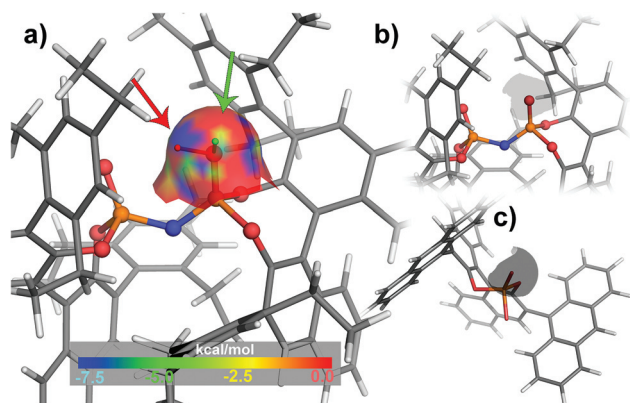


Fig. 10 (a) Map of the interactions of the anion of **cat-I** with an H⁺; (b) effective surface for the interaction with the substrate; (c) effective surface for **cat I**.

Notes and references

- 1 M. Terada, *Chem. Commun.*, 2008, 4097–4112.
- 2 G. Adair, S. Mukherjee and B. List, *Aldrichimica Acta*, 2008, **41**, 31–39.
- 3 M. Rueping, R. M. Koenigs and I. Atodiresei, *Chem. – Eur. J.*, 2010, **16**, 9350–9365.
- 4 A. Zamfir, S. Schenker, M. Freund and S. B. Tsogoeva, *Org. Biomol. Chem.*, 2010, **8**, 5262–5276.
- 5 J. Yu, F. Shi and L.-Z. Gong, *Acc. Chem. Res.*, 2011, **44**, 1156–1171.
- 6 M. Rueping, A. Kuenkel and I. Atodiresei, *Chem. Soc. Rev.*, 2011, **40**, 4539–4549.
- 7 T. Akiyama, *Chem. Rev.*, 2007, **107**, 5744–5758.
- 8 S.-L. You, *Chem. – Asian J.*, 2007, **2**, 820–827.
- 9 D. Parmar, E. Sugiono, S. Raja and M. Rueping, *Chem. Rev.*, 2014, **114**, 9047–9153.
- 10 T. Marcelli, P. Hammar and F. Himo, *Chem. – Eur. J.*, 2008, **14**, 8562–8571.
- 11 L. Simón and J. M. Goodman, *J. Am. Chem. Soc.*, 2008, **130**, 8741–8747.
- 12 T. Akiyama, H. Morita, P. Bachu, K. Mori, M. Yamanaka and T. Hirata, *Tetrahedron*, 2009, **65**, 4950–4956.
- 13 T. Marcelli, P. Hammar and F. Himo, *Adv. Synth. Catal.*, 2009, **351**, 525–529.
- 14 F.-Q. Shi and B.-A. Song, *Org. Biomol. Chem.*, 2009, **7**, 1292–1298.
- 15 L. Simón and J. M. Goodman, *J. Am. Chem. Soc.*, 2009, **131**, 4070–4077.
- 16 L. Simón and J. M. Goodman, *J. Org. Chem.*, 2010, **75**, 589–597.
- 17 S. Xu, Z. Wang, Y. Li, X. Zhang, H. Wang and K. Ding, *Chem. – Eur. J.*, 2010, **16**, 3021–3035.
- 18 C. Zheng, Y.-F. Sheng, Y.-X. Li and S.-L. You, *Tetrahedron*, 2010, **66**, 2875–2880.
- 19 P. Jain, H. Wang, K. N. Houk and J. C. Antilla, *Angew. Chem., Int. Ed.*, 2011, **51**, 1391–1394.
- 20 L. Simón and J. M. Goodman, *J. Org. Chem.*, 2011, **76**, 1775–1788.
- 21 M. N. Grayson and J. M. Goodman, *J. Am. Chem. Soc.*, 2013, **135**, 6142–6148.
- 22 X. Hong, H. B. Küçük, M. S. Maji, Y.-F. Yang, M. Rueping and K. N. Houk, *J. Am. Chem. Soc.*, 2014, **136**, 13769–13780.
- 23 K. Kanomata, Y. Toda, Y. Shibata, M. Yamanaka, S. Tsuzuki, I. D. Gridnev and M. Terada, *Chem. Sci.*, 2014, **5**, 3515–3523.
- 24 M. Terada, T. Komuro, Y. Toda and T. Korenaga, *J. Am. Chem. Soc.*, 2014, **136**, 7044–7057.
- 25 A. Kondoh, Y. Ota, T. Komuro, F. Egawa, K. Kanomata and M. Terada, *Chem. Sci.*, 2016, DOI: 10.1039/c5sc03175c.
- 26 F. Maseras, C. Liu and M. Besora, *Chem. – Asian J.*, 2015, DOI: 10.1002/asia.201501099.
- 27 P. Maity, R. P. Pemberton, D. J. Tantillo and U. K. Tambar, *J. Am. Chem. Soc.*, 2013, **135**, 16380–16383.
- 28 S.-S. Meng, Y. Liang, K.-S. Cao, L. Zou, X.-B. Lin, H. Yang, K. N. Houk and W.-H. Zheng, *J. Am. Chem. Soc.*, 2014, **136**, 12249–12252.
- 29 T. J. Seguin, T. Lu and S. E. Wheeler, *Org. Lett.*, 2015, **17**, 3066–3069.
- 30 I. Coric and B. List, *Nature*, 2012, **483**, 315–319.
- 31 J. H. Kim, I. Čorić, S. Vellalath and B. List, *Angew. Chem., Int. Ed.*, 2013, **52**, 4474–4477.
- 32 S. Liao, I. Čorić, Q. Wang and B. List, *J. Am. Chem. Soc.*, 2012, **134**, 10765–10768.
- 33 Y.-Y. Chen, Y.-J. Jiang, Y.-S. Fan, D. Sha, Q. Wang, G. Zhang, L. Zheng and S. Zhang, *Tetrahedron: Asymmetry*, 2012, **23**, 904–909.
- 34 K. Wu, Y.-J. Jiang, Y.-S. Fan, D. Sha and S. Zhang, *Chem. – Eur. J.*, 2013, **19**, 474–478.
- 35 D. An, Y.-S. Fan, Y. Gao, Z.-Q. Zhu, L.-Y. Zheng and S.-Q. Zhang, *Eur. J. Org. Chem.*, 2014, 301–306.
- 36 L. Liu, M. Leutzsch, Y. Zheng, M. W. Alachraf, W. Thiel and B. List, *J. Am. Chem. Soc.*, 2015, **137**, 13268–13271.
- 37 G. Jindal and R. B. Sunoj, *Angew. Chem., Int. Ed.*, 2014, **53**, 4432–4436.
- 38 Y. Y. Khomutnyk, A. J. Arguelles, G. A. Winschel, Z. Sun, P. M. Zimmerman and P. Nagorny, *J. Am. Chem. Soc.*, 2015, **38**, 444–456.
- 39 M. J. F., *et al.*, *Gaussian09, Revision B.01*, Gaussian, Inc., Wallingford CT, 2009.
- 40 M. Svensson, S. Humbel and K. Morokuma, *J. Chem. Phys.*, 1996, **105**, 3654–3661.
- 41 S. Dapprich, I. Komáromi, K. S. Byun, K. Morokuma and M. J. Frisch, *J. Mol. Struct.*, 1999, **461**, 1–21.
- 42 T. Vreven and K. Morokuma, *J. Comput. Chem.*, 2000, **21**, 1419–1432.
- 43 H. Zhao and D. G. Truhlar, *Theor. Chim. Acta*, 2007, **120**, 215–241.
- 44 Y. Zhao and D. G. Truhlar, *Acc. Chem. Res.*, 2008, **41**, 157–167.
- 45 R. Krishnan, J. S. Binkley, R. Seeger and J. A. Pople, *J. Chem. Phys.*, 1980, **72**, 650–654.
- 46 T. Clark, J. Chandrasekhar and P. v. R. Schleyer, *J. Comput. Chem.*, 1983, **4**, 294–301.
- 47 P. M. W. Gill, B. G. Johnson, J. A. Pople and M. J. Frisch, *Chem. Phys. Lett.*, 1992, **197**, 499–505.
- 48 A. K. Rappé, C. J. Casewit, K. S. Colwell, W. A. Goddard III and W. M. Skid, *J. Am. Chem. Soc.*, 1992, **114**, 10024–10035.
- 49 L. Simón and R. S. Paton, *J. Org. Chem.*, 2015, **80**, 2756–2766.
- 50 L. Simón and J. M. Goodman, *J. Am. Chem. Soc.*, 2012, **134**, 16869–16876.
- 51 N. Li, X.-H. Chen, J. Song, S.-W. Luo, W. Fan and L.-Z. Gong, *J. Am. Chem. Soc.*, 2009, **131**, 15301–15310.
- 52 M. N. Grayson, S. C. Pellegrinet and J. M. Goodman, *J. Am. Chem. Soc.*, 2012, **134**, 2716–2722.
- 53 R. S. Paton and J. M. Goodman, *J. Chem. Inf. Model.*, 2009, **49**, 944–955.
- 54 As has been described previously: (a) D. M. Hodgson, A. Charlton, R. S. Paton and A. S. Thompson, *J. Org. Chem.*,

1	2013, 78 , 1508–1518; (b) K. E. Jackson, C. L. Mortimer, B. Odell, J. M. McKenna, T. D. W. Claridge, R. S. Paton and D. M. Hodgson, <i>J. Org. Chem.</i> , 2015, 80 , 9838–9846. Python code available from https://github.com/bobbypaton/compchem .	59 M. Cossi, G. Scalmani, N. Rega and V. Barone, <i>J. Chem. Phys.</i> , 2002, 117 , 43–54.	1
5	55 S. Grimme, <i>Chem. – Eur. J.</i> , 2012, 18 , 9955–9964.	60 M. Cossi, G. Scalmani, N. Rega and V. Barone, <i>J. Comput. Chem.</i> , 2003, 24 , 669–681.	
	56 R. Cammi, B. Mennucci and J. Tomasi, <i>J. Phys. Chem. A</i> , 1999, 103 , 9100–9108.	61 A. V. Marenich, C. J. Cramer and D. G. Truhlar, <i>Phys. Chem. B</i> , 2009, 113 , 6378–6396.	5
10	57 R. Cammi, B. Mennucci and J. Tomasi, <i>J. Phys. Chem. A</i> , 2000, 104 , 5631–5637.	62 S. Grimme, J. Antony, S. Ehrlich and H. Krieg, <i>J. Chem. Phys.</i> , 2010, 132 , 154104.	
	58 M. Cossi, N. Rega, M. Scalmani and V. Barone, <i>J. Chem. Phys.</i> , 2001, 114 , 5691–5701.	63 <i>The PyMOL Molecular Graphics System, Version 0.99</i> , Schrödinger, LLC.	10
		64 A. R. Ionescu, A. Bérces, M. Z. Zgierski, D. M. Whitfield and T. Nukada, <i>J. Phys. Chem. A</i> , 2005, 109 , 8096–8105.	
15			15
20			20
25			25
30			30
35			35
40			40
45			45
50			50
55			55